Transferring the entatic state principle into copper photochemistry

B. Dicke,[1,2] A. Hoffmann,[3] J. Stanek,[3] M. S. Rampp,[4] B. Grimm-Lebsanft,[1,2] F. Biebl,[1,2] D. Rukser,[1,2] B. Maerz,[4] D. Göries,[5] M. Naumova,[1,6] M. Biednov,[1,2] G. Neuber,[1,2] A. Wetzel,[1,2] S. M. Hofmann,[4] P. Roedig,[5] A. Meents,[5] J. Bielecki,[7] J. Andreasson,[7,8,9] K. Beyerlein,[2] H. N. Chapman,[2,5] C. Bressler,[10,11, 12] W. Zinth,[4*] M. Rübhausen[1,2 *] and S. Herres-Pawlis[3*]

[1] *Institute of Nanostructure and Solid State Physics, University of Hamburg, 22761 Hamburg, Germany*

[2] *Center for Free-Electron Laser Science (CFEL), Luruper Chaussee 149, 22761 Hamburg, Germany*

[3] *Institute for Inorganic Chemistry, RWTH Aachen University, 52074 Aachen, Germany*

[4] *Institute for BioMolecular Optics and Center for Integrated Protein Science (CIPSM), Ludwig-Maximilians-Universität Munich, Oettingenstraße 67, 80538 Munich, Germany*

[5] *Deutsches Elektronensynchrotron (DESY), Notkestraße 85, 22607 Hamburg, Germany*

[6] *Department of Chemistry, University of Paderborn, 33098 Paderborn, Germany*

[7] *ELI Beamlines, Institute of Physics, Czech Academy of Science, Na Slovance 2, 182 21 Prague, Czech Republic*

[8] *Laboratory of Molecular Biophysics, Department of Cell and Molecular Biology, Uppsala University, Husargatan 3 (Box 596), SE-751 24 Uppsala, Sweden*

[9] *Condensed Matter Physics, Department of Physics, Chalmers University of Technology, Göteborg, Sweden*

[10] *European XFEL, Holzkoppel 4, 22869 Schenefeld, Germany*

[11] *Department of Physics, Technical University of Denmark, Fysikvej 307, Kongens Lyngby 2800, Denmark*

[12] *The Hamburg Center for Ultrafast Imaging, Universität Hamburg, Luruper Chaussee 149, 22761 Hamburg, Germany*

Abstract

The entatic state is a general principle in Nature which denotes the distortion of the coordination geometry of a regarded complex from its ideal-typical geometry with the target of lifting the energy levels of start and endpoint of reactions. By thus lowering the reorganisation energy of electron-transfer processes, the entatic state principle is crucial for a multitude of biochemical processes.

Here, we apply it to a copper complex with a specifically designed constraining ligand geometry, which exhibits very short ^{1}MLCT and ^{3}MLCT lifetimes. The guanidine-quinoline ligand acts on a bis(chelated) copper(I) centre, allowing only small structural changes after photoexcitation. By a multi-method approach using time-resolved UV/Vis, IR and X-ray absorption spectroscopy, time-resolved optical emission spectroscopy and by supporting density functional calculations on

the excited states we deliver a detailed picture of the structural dynamics on the picosecond to nanosecond time range. We hereby demonstrate that the entatic state principle is also valid to tune the photochemistry of copper complexes to allow fastest reaction speed.

Manuscript

The entatic state principle has been applied for 50 years to interpret thermally activated electron transfer processes at copper centres [1–10]. Entasis denotes a structural pre-distortion of a transition metal complex towards a reaction transition state, thus, facilitating a chemical reaction and, in a narrower sense, enabling faster electron transfer (Fig. 1a). This pre-distortion is also discussed as energisation of reactive states and is crucial for efficient catalysis in chemistry and biology [1,8,9]. Parallel to this development, photochemistry focuses on the elucidation of the excited state dynamics and reaction pathways[11–13]. Both concepts have yet not been combined, although especially in copper chemistry the entatic state principle and photochemical research have found vital applications, since copper is one of the most important redox-active metals playing a central role in several biological processes[14,15]. Tuning of the Cu(II/I) redox potential is crucial for efficient electron transfer in nature as well as for synthetic complexes in catalytic processes and in solar energy conversion[11,16]. The entatic state principle uses a preorganisation of the ligand sphere by a constrained geometry with high similarity for both oxidation states Cu(I) and Cu(II) [17]. Ligand preorganisation denotes the property of a ligand to stabilise a certain coordination mode and in same cases for a specific metal ion. This is different to the metal-ligand complementarity where the metal-ligand pair has an ideal geometrical and electronical fit. For a detailed discussion of the relation between the entatic state, ligand preorganisation and complementarity, see Ref. 17. The entatic state lowers the reorganisation energy during redox processes and, thus, facilitates them (Fig. 1a) [9,18,19]. For solar energy conversion schemes it is, however, desired to actually generate long-lived charge-separated states with sterically demanding ligand structures to enhance the current flow [11,20]. Therefore, the entatic state principle concerns both directions (to enhance and hamper charge transfer), since excited state lifetimes are susceptible towards substitution at specific ligand positions and can be tuned over two orders of magnitude by substitution exchange in acetonitrile [21,22].

In the context of the entatic state, intensive studies on conformationally invariant Cu(II/I) model complexes have been performed [23–27]. Very recently, Policar et al. developed a sugar-based

ligand, which provides a strong preorganisation for Cu(II) coordination in a trigonal bipyramid, but with an unusual stabilisation of its Cu(I) redox state [28]. Szymczak et al. synthesised a constrained Cu(I) complex, which is very close to a square-planar coordination[29]. Recently, we reported a series of bis(chelate) Cu(I) and Cu(II) guanidine-quinoline complex cations $[Cu^{II}(TMGqu)_2]^+$ and $[Cu^{I}(TMGqu)_2]^{2+}$ (see Figure 1b for overlay of both cations[10]). They display the astonishing feature that their structures are very similar possessing a coordination polyhedron in the middle between tetrahedral and square-planar environment [10]. A resonance Raman study of these Cu(I/II) complexes in solution showed that they come into resonance at nearly the same energy around ~3.5 eV by metal-to-ligand charge-transfer (MLCT) and ligand-to-metal charge-transfer (LMCT) processes [10]. We found a dominant Cu-N vibrational mode that couples the optical charge-transfer excitation with the distortion along the reaction coordinate leading from the more tetrahedral Cu(I) to a more flattened (towards square-planar coordination) Cu(II) geometry. The donor interplay between guanidine and quinoline units as well as the large steric encumbrance of guanidines were found to be crucial for this constrained coordination. These model compounds are extremely susceptible to MLCT and LMCT processes, as the predistortion lowers the energy barrier required to enable charge transfer.

In this work, we report on the dynamics of the structural and electronic changes as induced by an MLCT photoexcitation process utilising a collection of complementary experimental transient techniques, which provide crucial information on time scales covering more than four orders of magnitude. With time-resolved optical absorption and emission spectroscopy in the visible and UV range we identify short-lived electronic intermediate states. Time-resolved IR spectroscopy [30–33] characterizes these intermediates by probing the molecular vibrations in the ligand system. Finally, transient pump-probe X-ray absorption spectroscopy (XAS)[34–41] focuses on the changes of the Cu oxidation state and its coordination sphere in $[Cu^{I}(TMGqu)_2]^+$ following photoexcitation. The combination of these different experimental tools with extensive density functional theory (DFT) studies of the excited states and their spectroscopic features leads to a new comprehensive picture of the reaction dynamics involving excited singlet and - by intersystem crossing - triplet states.

Results and Discussion

As entatic state models, the guanidine-quinoline complexes $[Cu^{I}(TMGqu)_2]PF_6$ (**1**) and $[Cu^{II}(TMGqu)_2](OTf)_2$ (**2**)(Fig. 1b) consist of highly similar complex cations although containing Cu ions in different oxidation states (structural data reproduced in section 2 in the Supp.Information[10]). The UV/Vis spectra are dominated by the LMCT transition (quinoline-π* → Cu) of **2** at 390 nm versus the MLCT transition of **1** (Cu → quinoline/guanidine-π*) near 450 nm (Figure 1c) [10,42]. The static IR spectra (Figure 1d) of both complexes depict the key vibrations within the guanidine and quinoline units, which are highly sensitive towards the copper oxidation state. These differences will be used below to identify short-lived intermediate states. Hereby the most important bands are attributable to stretching vibrations of the guanidines, which are sensitive to the oxidation state of the copper centre. To monitor the MLCT dynamic processes in **1**, we use i) transient UV/Vis and IR spectroscopy allowing insights into the fast reaction dynamics directly after excitation up to 500 ps, while ii) time-resolved optical emission, and iii) X-ray absorption spectroscopy reach out to the longer nanosecond time scales. In addition, XAS delivers unique structural information on selected excited states which are directly correlated to density functional studies. All experimental and theoretical details can be found in the SI.

((please insert Figure 1 here))

Figure 1. a) Simplified illustration of the entatic state principle: Cu(II) has a clear electronic preference for square-planar coordination whereas Cu(I) does not have an electronically favoured coordination mode (d^{10} configuration) but is sterically mostly driven to tetrahedral motifs. The entatic state principle denotes an energisation of both states (here: misfit of ligands to square-planar and tetrahedral coordination) which leads to a smaller activation barrier.[9,17] The principle was developed for copper type-1 proteins but applies also to small molecule complexes with suited ligands [9]; b) overlay of the experimental structures of the cations of **1** and **2** (turqoise: copper, blue: nitrogen, black: carbon). The difference between the Cu(I) and Cu(II) oxidation states is expressed in a change of the angle between the CuN_2 planes by 20° and a shortening of the Cu-N_{gua} bond length by 0.1 Å [10]; c) static UV/Vis spectra of **1** (black) and **2** (red) in MeCN and d) static IR spectra (**1** in black and **2** in red) in CH_2Cl_2, gua = guandine related bands, qu = quinoline related bands.

Time-resolved optical absorption spectroscopy in the visible and IR

Information on the fast reaction dynamics is obtained from time-resolved optical absorption experiments, where **1** is excited with short pulses (90 fs) at λ_{exc} = 400 nm in its MLCT region. Figure 2a summarises the absorption difference spectra recorded in the UV/Vis range for a series

of delay times (width of the instrumental response function 150 fs). Directly after excitation, the ground-state absorption in the Cu(I) band decreases around 450 nm. A very broad absorption increase can be observed at longer wavelengths (480 - 730 nm) which we assign, supported by DFT calculations, to the formation of a quinoline radical anion upon MLCT[43]. At the small excitation energy of 400 nJ used in the experiment solvated electrons do not show up (see section 3 of the Supp. Information). The dip in the 530 nm range could originate from stimulated emission from the excited states (Fig. 2b).

The amplitudes of the transient difference spectra show a reduction by ca. 50% during the first 5 ps, after which a decay on the 100 ps timescale takes over. A global analysis of the time dependent absorption with exponential functions yields four time constants: τ_1=0.2 ps, τ_2=1.3 ps, τ_3=11 ps, τ_4=120 ps. The corresponding fit amplitudes (Supplementary Figure 2) contain information on the related reactions. Light absorption inducing an optical (d^{10}-π^*) transition populates the electronically excited and symmetry-allowed $\mathbf{S_{14}}$ state (obtained by TD-DFT, see SI) (Figure 3). Within our time resolution the initial reaction dynamics [11] lead to the $\mathbf{S_1}$ state which subsequently relaxes the nuclear coordinates to $\mathbf{S_{1,relax}}$ within τ_1=0.2 ps. In the τ_2=1.3 ps reaction the absorption signal decays by ca. 50%. The shape of the corresponding amplitudes is consistent with a partial Cu(II) to Cu(I) back-reaction. After a transient with weak amplitudes (τ_3 = 11 ps) the remaining absorption signal essentially vanishes with τ_4 = 120 ps reforming the original Cu(I)-type ground state of **1** in this process. Complementary information on the lifetimes of excited electronic states is obtained from time-resolved optical emission spectroscopy revealing a time constant in the 100 to 200 ps range (Supplementary Figure 16).

More details on the nature of the involved states are obtained from transient IR experiments probing ligand vibrations (Fig. 2c, width of the instrumental response function 1.5 ps). The transient difference spectra recorded at early times suggest that the original ground state absorption vanishes upon excitation, while a new species with Cu(II) character is formed (positive bands at 1400 and 1510 cm^{-1} directly related to guanidine vibrational shift due to Cu(II) character, assigned by DFT, see section 4 of the Supp. Information). Global modelling with three time constants, (τ_2= ~2 ps , τ_3=11 ps and τ_4=120 ps) delivers interesting information about the transient species. The fit amplitudes (Supplementary Figures 2-9) show that both, the τ_2 and the τ_4 related processes are due to a back-reaction from a state with Cu(II) character to a Cu(I) state (for detailed discussion of τ_2 vide infra). The amplitudes of the τ_3 component show the decay of

red-shifted absorption combined with bleach recovery of ground state bands, i.e. features expected for cooling of a vibrationally hot ground state of **1**.[44] Hence, two decay channels exist for $\mathbf{S_{1,relax}}$: into the hot ground state and into the triplet state $\mathbf{T_1}$ (Fig. 3), which returns with a longer τ_4 constant into the Cu(I) ground state. The analysis of the time-resolved UV/Vis and IR absorption experiments indicate that very little absorption changes persist at later times (>500 ps). Thus not much more than ~5% of the excited complexes may follow other decay paths, e. g. via long-lived triplet states.

Additional measurements with time-resolved optical absorption spectroscopy (see section 3 in Supp. Information) were performed on samples dissolved in dichloromethane (DCM). These results follow the same reaction scheme described above with a slower time constant in DCM of τ_4=240ps than in CD_3CN τ_4=120ps. UV/Vis experiments with the excitation wavelength λ_{exc2}=320 nm in DCM yielded no systematic differences of the time-dependent absorption changes in the picosecond time range indicating no change in reaction pathway for excitation energies in the 3.1 eV and 3.87 eV range (Table 4).

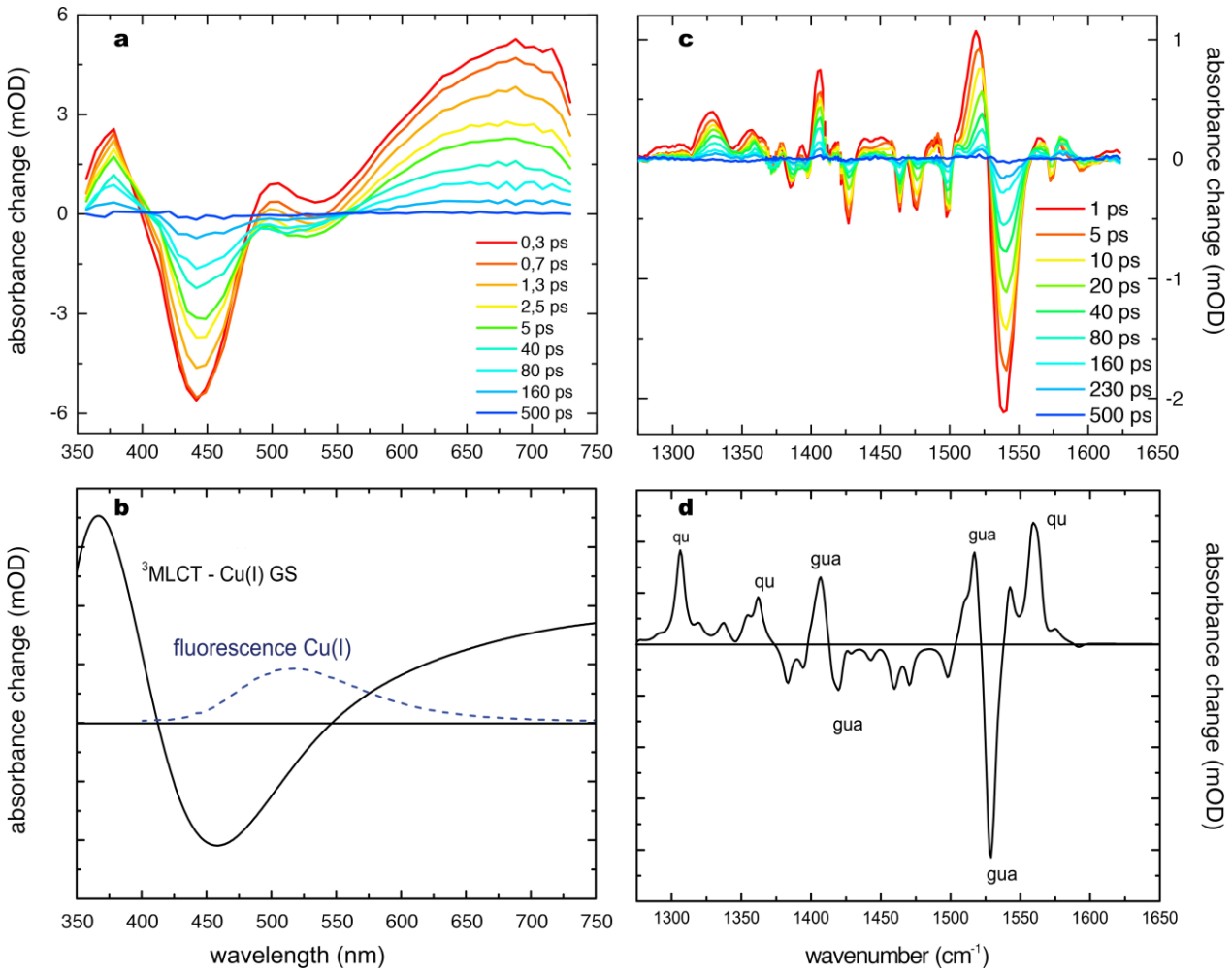

Figure 2. a) and c) Transient UV/Vis and IR difference spectra in MeCN or d_3-MeCN; excitation at 400 nm. b) calculated UV/Vis difference spectra ^{3}MLCT – Cu(I) GS (B3LYP/def2-svp) including the qualitative emission spectrum (dashed). d) calculated IR difference spectra ^{3}MLCT – Cu(I) GS of the triplet state (B3LYP-D3/def2-tzvp, PCM).

The time-resolved experiments performed in the IR and UV/Vis lead to the molecular reaction scheme of Figure 3. Light absorption initially populates a high lying Franck-Condon state $\mathbf{S_{14}}$ with MLCT-character, which relaxes rapidly (τ_1=0.2 ps) by internal conversion [45] to a state $\mathbf{S_{1,relax}}$ with the following spectroscopic properties: (i) strong bleach of the original absorption bands of **1**, (ii) a broad absorption extending from the blue part of the spectrum to the near IR, (iii) a pronounced absorption band around 500 nm, (iv) IR signatures showing formation of Cu(II)-guanidine-quinolinyl radical bands. The different spectral features together with DFT calculations support that $\mathbf{S_{1,relax}}$ is the ^{1}MLCT state with Cu(II) and a quinolinyl radical anion. With the time constant of τ_2=~2 ps there is a strong decay of the excited state amplitude and the formation of a vibrationally hot Cu(I) species. Its subsequent cooling (11 ps) suggests that about

50% of the population in state $\mathbf{S_{1,relax}}$ decays to a vibrationally hot ground state of **1**. The remaining population reacts further to another electronically excited state with Cu(II)-character, named $\mathbf{T_1}$, with new properties. A comparison of the amplitude spectra and the calculated IR-difference spectra for the $\mathbf{T_1}$ state and species **1** (Fig. 2d) strongly suggests that $\mathbf{T_1}$ is indeed a ^{3}MLCT state. Moreover, the calculated UV spectrum for $\mathbf{T_1}$ exhibits UV absorption at 400 nm (as observed in the transient UV) together with a broad absorption at 600 nm, the latter being assigned to transitions within the quinolinyl radical (Fig. 2b). The bifurcation out of $\mathbf{S_{1,relax}}$ towards the hot ground state and the excited state $\mathbf{T_1}$ is guided by the respective rates $1/\tau_{2a}$ and $1/\tau_{2b}$. The final process for $\mathbf{T_1}$ is its decay (τ_{4a}=120 ps) to the reactant state **1**. Further long-lived states with small amplitude observed in the emission experiment can be related to a solvent exciplex $\mathbf{T_{1,MeCN}}$ as discussed in more detail below.

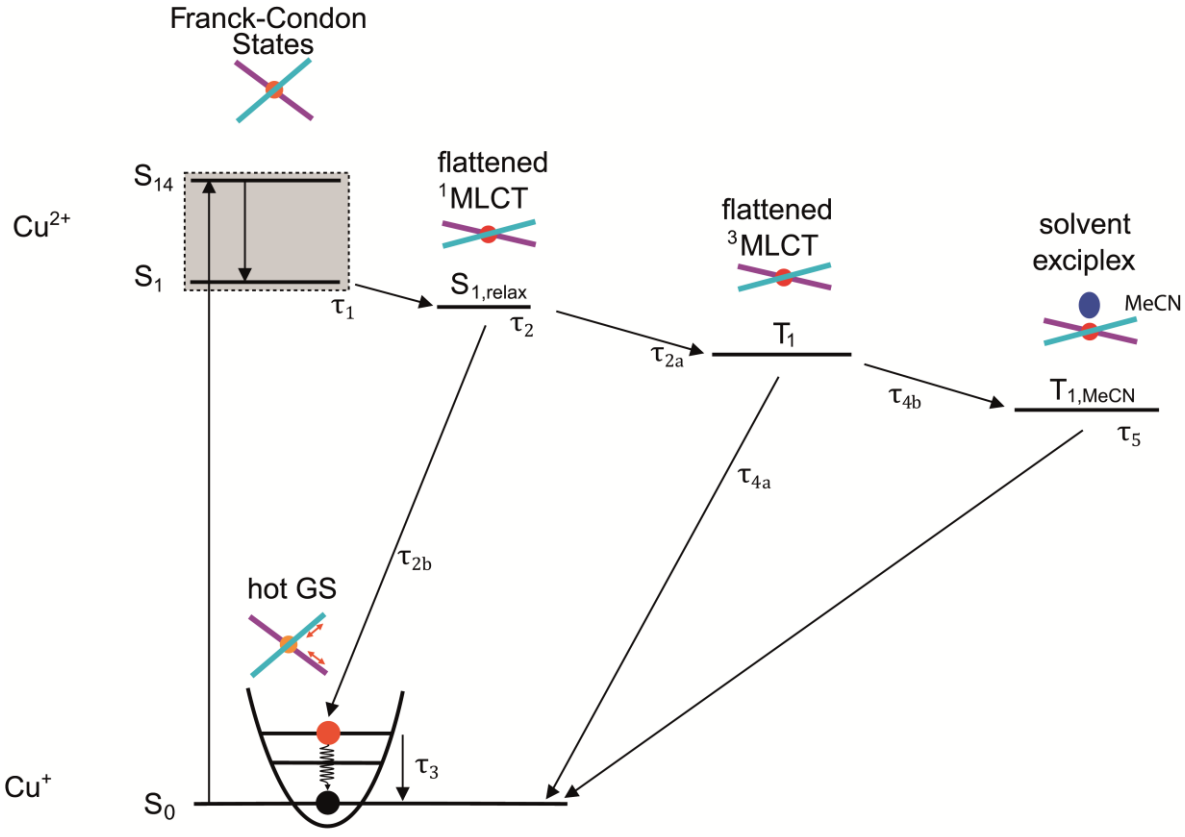

Figure 3. Schematic representation of the involved states (assignment by TD-DFT, see section 6 of the Supp. Information). The coloured scheme illustrates the angle between the ligand planes in the bis(chelate) complexes.

Table 1. Overview of all measured decay times determined by combining different experimental techniques. *For the determination of τ_{4b} and τ_5 , τ_{4a} was set to 120 ps as measured by TR UV/Vis

and TR IR. The time constants τ_{4b} and τ_5 were derived from the fluorescence signal as it offers better signal to noise compared to XAS. Time delay curves between XAS and TR emission are identical (see Fig. 4d)

Method	λ_{pump} (nm)	Solvent	τ_1 ps	τ_2 ps	τ_3 ps	τ_{4a} ps	τ_{4b} ps	τ_5 ps	Indication
TR UV/Vis	400	MeCN	0.2 ±0.05	1.30 ±0.4	11.00 ±5	120 ±20	-	-	Electronic states
	320	DCM	0.4±0.1	2.2. ±0.5	17 ±8	240 ± 30	-	-	
	400	DCM	0.4±0.1	2.1±0.5	20 ±8	260 ±30	-	-	
TR IR	400	MeCN	-	2 ±1.5	11 ±3	120 ±20	-	-	Ligand vibrations indicating oxidation states
TR PP XAS	343	MeCN	-	-	-	120*	1222 ± 40	1876± 76	Oxidation state, Cu-N distances
TR emission	410	MeCN	-	-	-	120*	1222 ± 40	1876± 76	Electronic states

$1/\tau_2 = 1/\tau_{2a} + 1/\tau_{2b}$. Amplitudes in the DADS (see SI, Figure S2) indicate that $\tau_{2a} \approx \tau_{2b}$, thus τ_{2a} and τ_{2b} are estimated to app. 2.6 ps; $1/\tau_4 = 1/\tau_{4a} + 1/\tau_{4b}$,

Pump probe XAS

To obtain more insight into the nature of the ^{3}MLCT state, pump-probe XAS experiments can measure the oxidation state of Cu via X-ray absorption near edge spectroscopy (XANES). In addition, the extended X-ray absorption fine structure (EXAFS) is capable to determine structural changes around the Cu centre [34–40]. Copper K-edge XAS spectra of **1** (red), **2** (black) and of the optically generated triplet $\mathbf{T_1}$ (green) are shown in Fig. 4a after 100 ps. The measured pumped XAS spectrum $\mathbf{1_{pumped}}$ is a superposition of ground state species **1** and excited state species $\mathbf{T_1}$ via

$$A(\boldsymbol{T_1}) = \left[A(\mathbf{1}_{pumped}) - \mathrm{A}(\mathbf{1})\right] \cdot f^{-1} + A(\mathbf{1}) \quad \textbf{(eq1),}$$

where f denotes the photoexcited fraction of excited state molecules. By scaling the experimental transient difference spectrum $\left[A(\mathbf{1}_{pumped}) - \mathrm{A}(\mathbf{1})\right] \cdot with\ f^{-1}$ to match the static difference spectrum $A(\mathbf{2}) - A(\mathbf{1})$ we extract f ~10% (Fig. 4b), since the XANES spectra of **2** and $\mathbf{T_1}$ are very similar. It is notable that both species have the absorption edge blue-shifted by ca. 2.5 eV with respect to the XANES of the reactant **1** (Fig. 4a), which is indicative for a Cu species with oxidation state II. Fig. 4c zooms into the pre-edge area where 1s → 3d+4p transitions[46] indicate the $3d^9$ configuration of Cu(II). Each of these two observations thus confirm the Cu(II) character of the transiently formed MLCT state [37]. Furthermore the XAS spectra of **2** and of $\mathbf{T_1}$ show for higher energies of about 9050 eV a shift of the first resonance peak with respect to the reactant **1** spectrum (Figure 4b). This shift is related to the expected structural distortion between Cu(I) and

Cu(II) complexes which involves a length contraction of the Cu-N_{gua} bonds. At energies far above the edge (in the 30-1000 eV region) the EXAFS provides information on interatomic distances next to type and number of scattering atoms around the selected absorber [47,48,49] (see section 4 of the Supp. Information for details). The first coordination shell around Cu for the photoexcited complex $\mathbf{T_1}$ is closer than for the reactant **1**, by ΔR(Cu-N) = -0.070 ± 0.044 Å from the reactant Cu-N distance of R(Cu-N) = 2.024 ± 0.021 Å, in agreement with our DFT-results for both groups of ligand atoms ΔR(Cu-N_{gua}) = -0.09 Å and ΔR(Cu-N_{qu}) = -0.08 Å.

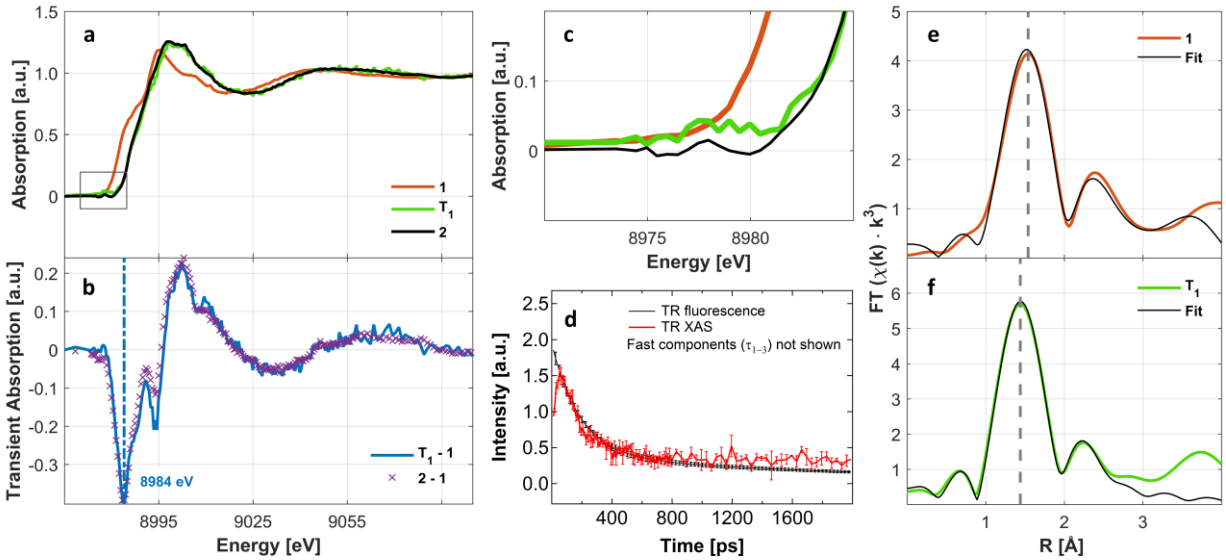

Figure 4. a) K-edge XAS spectra of **1** (red curve), of **2** (black curve) and of $\mathbf{T_1}$ for an ideal delay (green curve). b) corresponding transient difference spectra **2 - 1** (purple x-symbols) and $\mathbf{T_1}$ **- 1** (blue curve). c) pre-edge region of a). d) XAS transient difference signal between $\mathbf{T_1}$ **- 1** as function of time delay at a fixed energy of 8984 eV (red points including error bars). This energy corresponds to the strongest transient signal as indicated by the vertical line in b). The black curve represents the TR fluorescence at 510 nm emission up to 2 ns. e) and f) Fourier transform amplitudes of the EXAFS as function of the radial distance for **1** and $\mathbf{T_1}$. The spectra clearly show the difference in bond distance within the first coordination shell of **1** and $\mathbf{T_1}$ as marked by the dashed vertical lines. In detail the EXAFS fits of **1** and $\mathbf{T_1}$ reveal a bond length change of the mean Cu-N distances of -0.070 Å ± 0.044 Å upon the photoexcitation.

The time dependence of the XAS signal at 8984 eV, the position of largest difference to the Cu(I) ground state, is shown in Figure 4d (red points and error bars). It allows the analysis of the temporal decay of the involved excited states. We also plot the transient fluorescence emission at 510 nm up to 2 ns (black curve). With regard to Table 1, all data sets agree well with each other for the 120 ps feature considering the involved error bars. The fit to a model where the initial decay represents the two depopulation channels of $\mathbf{T_1}$ into **1** with τ_{4a} and of $\mathbf{T_1}$ into $\mathbf{T_{1,MeCN}}$ with

τ_{4b} is shown in the SI and the results are given in Table 1. $\mathbf{T_{1,MeCN}}$ is another MLCT-Cu(II) component of smaller amplitude decaying in the ns time domain, which is related to the formation of an exciplex (details see section 6 of the Supp. Information).

The observed Cu-N bond length shortening in $\mathbf{T_1}$ is caused by the fact that the former HOMO of **1** had Cu-N antibonding character[42] (see also Supplementary Fig. 19 of the β-LUMO of $\mathbf{T_1}$). Excitation of an electron from the HOMO to a quinolinyl π* orbital relieves the antibonding pressure thus enabling the bond length decrease.

During formation of the $\mathbf{S_{1,relax}}$ state within a few hundred fs the structural reorganisation at the copper takes place. Since $\mathbf{S_{1,relax}}$ and $\mathbf{T_1}$ are geometrically rather similar and the corresponding spin orbitals of $\mathbf{S_1}$ and $\mathbf{T_1}$ (Supplementary Figures 19 and 21) are twisted against each other, the spin-orbit coupling (SOC) is relatively large and the intersystem crossing (ISC) is completed within 2 ps which is fast for an ISC process at Cu [11,51]. Tahara et al. reported for the ISC values of 8-10 ps for substituted phen complexes $[Cu(dmphen)_2]^+$ and $[Cu(dpphen)_2]^+$.[13] Without substitution, no ISC is observed but a direct transition to the GS in 1.8 ps.[13] Figure 5 summarises the observed changes on both reaction coordinates, i) angle between the chelate planes and ii) Cu-N_{gua} bond length. The reaction path from the Franck-Condon $\mathbf{S_1}$ state over $\mathbf{S_{1,relax}}$ into $\mathbf{T_1}$ benefits from the entatic state principle, since both extremes of the reaction coordinate (**1** and **2** in their ground states) are structurally rather similar through the energisation by the ligands. The large amount of covalency of the guanidine-Cu bond as well as the structural constraint lower the degree of potential "flattening" of $\mathbf{S_{1,\,relax}}$ and $\mathbf{T_1}$ (implication of the entatic state!) and lead to the rotation of the corresponding orbital required for efficient SOC.[52]

$\mathbf{T_1}$ in turn decays to the ground state rather fast in 120 ps by a back-transfer of the electron from the formally reduced ligand to the copper ion. This is again at the lower end for ISCs [11] and can be traced back to the fact that $\mathbf{T_1}$ geometrically strongly ressembles **2** and **1** with an efficient SOC and corresponding orbital rotation (Supplementary Figure 21). Tahara et al. reported values in the ns range for this transition.[13] We propose that this fast ISC can be correlated with the small HOMO-LUMO gap of ~0.37 eV which is in accordance with literature results and caused by the large spin-orbit coupling [50]. This would imply that the entatic state principle is also applicable for spin state control. A direct connection between spin state control and the entatic state has recently been reported for iron enzymes by Solomon et al.[53]

Normally, the entatic state principle is valid for ground-state processes which belong to the classical region of Marcus theory.[18,27] Contrastingly, MLCT processes are often Marcus-inverted processes. However, in the present case, the free energy of the $\mathbf{T_1}$ decay is considerably smaller than the reorganisation energy (details see section 6 of Supp. Information). Consequently, the $\mathbf{T_1}$ decay can be treated as normal Marcus process.

Hence, we propose that the entatic state principle is not only valid for electron transfer steps themselves, but also for optically excited charge-transfer processes. Since the complexes are restrained by their ligands, their excited states are restrained as well to attain the ground state in due course. This can be regarded as a contrasting effect to that observed in complexes with large substituents, which enforce long triplet lifetimes of up to ns[11].

((please insert Figure 5 here))

Figure 5. centre: Two-dimensional reaction coordinate of the excitation of **1** and the subsequent decay. One axis depicts the angle between the coordination plane CuN_2 of one chelate ligand versus the coordination plane CuN_2` of the other chelate ligand (see inset on the right side), hence indicating the degree of torsion between square planar (=0°) and tetrahedral (=90°) configuration. GS: ground state. The entatic state principle applies for the relaxation of $\mathbf{S_1}$ to $\mathbf{S_{1,relax}}$, to the ISC from $\mathbf{S_{1,relax}}$ to $\mathbf{T_1}$ and to the final electron-backtransfer from $\mathbf{T_1}$ to $\mathbf{S_0}$. The red inset illustrates the entatic state principle for the diagonalised slice of the diagram (red inset slightly adapted from ref. 10 for reasons of clarity).

Summary

The energisation of Cu(I) and Cu(II) complexes by tailored guanidine-quinoline ligands realises the entatic state principle. Herein, we document the impact of the entatic state principle on their photochemical behaviour. The use of complementary experimental techniques allows an understanding of the electronic charge transfer processes in the copper quinoline-guanidine complexes from the perspective of the electronic system, the structural degrees of freedom of copper, and the ligands. Transient absorption and fluorescence spectroscopy deliver all relevant electronic time scales whereas transient IR spectroscopy provides information on structural distortions of the ligand. XAS gives insight into the change of the copper oxidation state and of the first coordination shell. The geometric restraints of the copper(I) guanidine complex lead to very fast structural dynamics since all involved states are structurally rather similar owing to the preorganisation of the metal coordination by the ligand. This example demonstrates for the first

time that the entatic state principle is highly valuable for photochemistry. In order to further expand the underlying concept to provide an explanation for tunable fast spin state control new experiments exploiting ultrafast x-ray emission spectroscopy would be desired, which can reliably monitor spin states in transition metal complexes.

Materials and methods

All materials and methods are described in detail in the Supporting Information.

All manipulations involving air- and moisture-sensitive compounds were performed under pure dinitrogen (N_2), dried over granulate P_4O_{10}, using Schlenk techniques, or in a glovebox with dried solvents. Solvents were either distilled from sodium benzophenone ketyl radical (THF, $C_2H_5OC_2H_5$) or from CaH_2 (CH_3CN, CD_3CN, CH_2Cl_2). The complexes were synthesised according to published procedures[10].

The ultrafast absorption changes from the IR to the UV are measured in excite and probe experiments based on a laser-amplifier system ((Spitfire Pro, Tsunami, Spectra Physics, repetition rate 1 kHz). For details see Supporting Information section Time-resolved absorption measurements. Excitation pulses at 400 nm are obtained via second harmonic generation. Probing pulses in the visible and near UV are produced by continuum generation in CaF_2. Probing in the mid-IR uses pulses generated by non-collinear and collinear optical parametric amplifiers and difference frequency mixing in an AgGaS2 nonlinear crystal.

Excitation and properly delayed probing pulses are overlaid in optical cells containing the sample molecules in solution. The Cu-compounds are pumped through the cells to exchange the excited volume between two subsequent excitation pulses. The transmission of the sample was recorded using spectrographs in combination with multichannel array detectors (MCT IR-0144, Infrared Systems Development for the mid-IR and S3902-512Q from Hamamatsu for the UV and the visible). The temporal resolution was ca. 100 fs for UV/vis and 1.5 ps for the IR probing experiment. For each delay time position ca. 10.000 shots were averaged and the excitation induced absorption changes are calculated from measurements with and without excitation pulses. The measurements are performed under magic angle conditions and at room temperature.

The transient absorption spectra were globally fitted with exponential functions leading to the decay times τ_k and the decay associated difference spectra (DADS) of the intermediate states.

For the fluorescence experiments a Tsunami Ti:Sapphire laser system, model HP fs 15 W P in conjunction with a pulse picker, model 3980-2S (all Spectra Physics Lasers Inc., California) with an integrated frequency doubler was used. The repetition rate was set to 8 MHz and the laser power in the range of up to 10 mW. For TCSPC a PicoQuant PMT Hybrid 06 detector was used. For steady state measurements a thermo-electrically cooled QE65000 spectrometer (Ocean Optics, Florida) was used. For the measurements a Suprasil glass cuvette (Hellma Analytics, Müllheim, Germany) was filled with 3 ml solution. The PMT was connected to a PicoQuant TimeHarp260P single photon counting PCI express card.

The TR PP XAS experiments were performed at beam line P11 of the PETRA III synchrotron light source at Deutsches Elektronen Synchrotron (DESY). PETRA III was operating in 40 bunch mode with a time gap of 192ns between two adjacent bunches and a bunch revolution frequency of 130 kHz. The sample was pumped into an excited state by a femtosecond PHAROS laser (Light conversion Ltd., Lithuania) at 343 nm and probed by an X-ray pulse.

To prevent radiation damage a liquid micro-jet system was used for sample delivery. The thickness of the jet was between 150 μm to 300 μm. The temporal overlap of laser and X-ray pulses was assured via a fast photo diode located at the jet position. To obtain the XAS spectra X-ray fluorescence yield mode was used with an avalanche photo diode (model APD001 from FMB Oxford) in 90° configuration. A second APD for normalization was directed towards a metal foil located several centimetres behind the sample position. The acquisition rate was set to 130 kHz which is twice the repetition rate of the laser system of 65 kHz. The used digitizer (Model ADQ412AC, 12 bit, 2/4GS, SP Devices) allowed to register multi-photon events thus drastically improving the signal-to-noise ratio.

For the quantum chemical calculations of the excited states, B3LYP/def2-svp was used as density functional method. The key geometric data of the symmetry-allowed singlet excitations are summarized in Supplementary Table 5. The reorganisation energy of the ISC can be described as the sum of reorganisation energies of the corresponding S_0 and T_1 ion pair. The reorganisation energy of each cation can be calculated by its optimised ground state energy and the single point energy of i.e. a singlet configuration in the ligand environment of the corresponding T_1 complex (denoted as SingL(Trip)) (Supplementary Equation 4 and Supplemenatry Figure 23).

Author contributions

B.D., M. N., M.B., B.G.-L., S.H.-P., A.H., J.S., D.R., A.W., and J. B. performed the transient XAS measurements, which were under supervision of M.R. The setup for transient XAS measurements was designed and developed by D.G., B. D., P. R. and A. M. C.B., B.D., D.G., S.H.-P. and M.R. contributed to the improved data acquisition technique. B.D. and M.N. analysed the transient XAS data. B.G.-L. performed the time-resolved optical emission experiments under supervision of M.R. J.A., F.B., H.C., K.B. and G. N. participated in the discussions about the data. A.H. and J. S. prepared the samples and A.H. performed the DFT calculations. The interpretation of the theoretical data in relation to the diverse experimental data was done by A.H. and S.H.-P.. M.S.R. and S.M.H. performed the transient IR measurements under the supervision of W.Z. B.M. accomplished the transient UV/Vis measurements under the supervision of W.Z.. The interpretation of the entire experimental optical and XAS data was delivered by CB, MR, SHP, and WZ. S.H.-P., W.Z., and M.R. designed the study and wrote the manuscript together with CB, A.H. and B.D.

Acknowledgements

S.H.-P. acknowledges generous funding by the Deutsche Forschungsgemeinschaft (FOR1405 and SFB749, project B10) and M.R. thanks the Bundesministerium für Bildung und Forschung (BMBF VUV-FAST/05K2014 und 05K12GU1) and DFG (FOR1405). Moreover, W.Z. thanks the SFB749 (project A5) and the Cluster of Excellence 'Munich-Center for Advanced Photonics' and 'Center for Integrated Protein Science (CIPSM)'. This work was supported by the project ELI - Extreme Light Infrastructure – phase 2 (CZ.02.1.01/0.0/0.0/15_008/0000162) from European Regional Development Fund. J.A. acknowledges funding from the Röntgen Ångström Cluster and Chalmers Area of Advance Materials Science. C.B. is grateful for funding by the European XFEL, the DFG via SFB925 (TP A4), and the Centre for Ultrafast Imaging. Parts of this research were carried out at beamline P11 at the PETRA III storage ring at DESY, a member of the Helmholtz Association (HGF). We thank the DESY beamline scientists B. Reime, A. Burkhardt, S. Panneerselvam, and O. Lorbeer for their support. Moreover, we thank the XFEL team members C. Youngman, P. Gessler, A. Beckmann, and A. Galler for the efficient integration of the MHz digitizer into our X-ray setup at P11.

References (at maximum 50)

1. Vallee, B. L. & Williams, R. J. P. Metalloenzymes: The entactic nature of their active sites. *Proc. Natl. Acad. Sci. U. S. A.* **59,** 498–505 (1968).

2. Williams, R. J. P. Energised (entatic) states of groups and of secondary structures in proteins and metalloproteins. *Eur. J. Biochem.* **234,** 363–381 (1995).

3. Williams, R. J. P. Catalysis by metallo-enzymes: The entatic state. *Inorg. Chim. Acta Rev.* **5,** 137–155 (1971).

4. Gray, H. B. & Malmström, B. G. Long-range electron transfer in multisite metalloproteins. *Biochemistry* **28,** 7499–7505 (1989).

5. Malmström, B. G. Rack-induced bonding in blue-copper proteins. *Eur. J. Biochem.* **223,** 711–718 (1994).

6. Comba, P. Strains and stresses in coordination compounds. *Coord. Chem. Rev.* **182,** 343–371 (1999).

7. Lancaster, K. M., DeBeer George, S., Yokoyama, K., Richards, J. H. & Gray, H. B. Type-zero copper proteins. *Nat. Chem.* **1,** 711–715 (2009).

8. Comba, P. *et al.* A Bispidine Iron(IV)-Oxo Complex in the Entatic State. *Angew. Chem. Int. Ed.* **55,** 11129–11133 (2016).

9. Comba, P. Coordination compounds in the entatic state. *Coord. Chem. Rev.* **200–202,** 217–245 (2000).

10. Hoffmann, A. *et al.* Catching an entatic state - a pair of copper complexes. *Angew. Chem. Int. Ed.* **53,** 299–304 (2014).

11. Mara, M. W., Fransted, K. A. & Chen, L. X. Interplays of excited state structures and dynamics in copper(I) diimine complexes: Implications and perspectives. *Coord. Chem. Rev.* **282–283,** 2–18 (2015).

12. Hua, L., Iwamura, M., Takeuchi, S. & Tahara, T. The substituent effect on the MLCT excited state dynamics of Cu(I) complexes studied by femtosecond time-resolved absorption and observation of coherent nuclear wavepacket motion. *Phys. Chem. Chem. Phys.* **17,** 2067–77 (2015).

13. Iwamura, M., Takeuchi, S. & Tahara, T. Ultrafast Excited-State Dynamics of Copper(I) Complexes. *Acc. Chem. Res.* **48,** 782–791 (2015).

14. Solomon, E. I. *et al.* Copper active sites in biology. *Chem. Rev.* **114,** 3659–3853 (2014).

15. Solomon, E. I. & Hadt, R. G. Recent advances in understanding blue copper proteins. *Coord. Chem. Rev.* **255,** 774–789 (2011).

16. Choi, M. & Davidson, V. L. Cupredoxins - a study of how proteins may evolve to use metals for bioenergetic processes. *Metallomics* **3,** 140–51 (2011).

17. Comba, P. & Schiek, W. Fit and misfit between ligands and metal ions. *Coord. Chem. Rev.* **238–239,** 21–29 (2003).

18. Rorabacher, D. B. Electron transfer by copper centers. *Chem. Rev.* **104,** 651–697 (2004).

19. Gray, H. B., Malmström, B. G. & Williams, R. J. P. Copper coordination in blue proteins. *J. Biol. Inorg. Chem.* **5,** 551–559 (2000).

20. Bergmann, L., Hedley, G. J., Baumann, T., Bräse, S. & Samuel, I. D. W. Direct

observation of intersystem crossing in a thermally activated delayed fluorescence copper complex in the solid state. *Sci. Adv.* **2,** 1–6 (2016).

21. Lockard, J. V. *et al.* Influence of ligand substitution on excited state structural dynamics in Cu(I) bisphenanthroline complexes. *J. Phys. Chem. B* **114,** 14521–14527 (2010).

22. Kohler, L. *et al.* Synthesis, structure, ultrafast kinetics, and light-induced dynamics of CuHETPHEN chromophores. *Dalton Trans.* **45,** 9871–9883 (2016).

23. Hancock, R. D. & Martell, A. E. Ligand design for selective complexation of metal ions in aqueous solution. *Chem. Rev.* **89,** 1875–1914 (1989).

24. Knapp, S. *et al.* Nearly tetrahedral 1:2 complexes of copper(I), copper(II), nickel(II), cobalt(II), and zinc(II) with 2,2'-bis(2-imidazolyl)biphenyl. *J. Am. Chem. Soc.* **109,** 1882–1883 (1987).

25. Comba, P., Kerscher, M. & Roodt, A. Slow electron self-exchange in spite of a small inner-sphere reorganisation energy - the electron-transfer properties of a copper complex with a tetradentate bispidine ligand. *Eur. J. Inorg. Chem.* 4640–4645 (2004).

26. Xie, B., Elder, T., Wilson, L. J. & Stanbury, D. M. Internal reorganization energies for copper redox couples: The slow electron-transfer reactions of the [Cu II/I $(bib)_2$ $]^{2+/+}$ couple. *Inorg. Chem.* **38,** 12–19 (1999).

27. Chaka, G. *et al.* A definitive example of a geometric 'entatic state' effect: Electron-transfer kinetics for a copper(ll/l) complex involving a quinquedentate macrocyclic trithiaether - Bipyridine ligand. *J. Am. Chem. Soc.* **129,** 5217–5227 (2007).

28. Garcia, L. *et al.* Entasis through hook-and-loop fastening in a glycoligand with cumulative weak forces stabilizing Cu^{I}. *J. Am. Chem. Soc.* **137,** 1141–1146 (2015).

29. Dahl, E. W. & Szymczak, N. K. Hydrogen bonds dictate the coordination geometry of copper: characterization of a square-planar copper(I) complex. *Angew. Chem. Int. Ed.* **55,** 3101–3105 (2016).

30. Bucher, D. B., Pilles, B. M., Carell, T. & Zinth, W. Charge separation and charge delocalization identified in long-living states of photoexcited DNA. *Proc. Natl. Acad. Sci. U. S. A.* **111,** 4369–4374 (2014).

31. Vos, M. H. & Liebl, U. Time-resolved infrared spectroscopic studies of ligand dynamics in the active site from cytochrome c oxidase. *Biochim. Biophys. Acta* **1847,** 79–85 (2015).

32. Poynton, F. E. *et al.* Direct observation by time-resolved infrared spectroscopy of the bright and the dark excited states of the $[Ru(phen)_2(dppz)]^{2+}$ light-switch compound in solution and when bound to DNA. *Chem. Sci.* **7,** 3075–3084 (2016).

33. Hall, J. P. *et al.* Monitoring one-electron photo-oxidation of guanine in DNA crystals using ultrafast infrared spectroscopy. *Nat. Chem.* **7,** 961–967 (2015).

34. Gawelda, W. *et al.* Electronic and molecular structure of photoexcited $[Ru^{II}(bpy)_3]^{2+}$ probed by picosecond x-ray absorption spectroscopy. *J. Am. Chem. Soc.* **128,** 5001–5009 (2006).

35. Bressler, C. *et al.* Towards structural dynamics in condensed chemical systems exploiting ultrafast time-resolved x-ray absorption spectroscopy. *J. Chem. Phys.* **116,** 2955–2966 (2002).

36. Bressler, C. & Chergui, M. Molecular structural dynamics probed by ultrafast x-ray absorption spectroscopy. *Annu. Rev. Phys. Chem.* **61,** 263–282 (2010).

37. Mara, M. W. *et al.* Effects of electronic and nuclear interactions on the excited-state properties and structural dynamics of copper(I) diimine complexes. *J. Phys. Chem. B* **117,** 1921–1931 (2013).

38. Chen, L. X. Probing transient molecular structures in photochemical processes using laser-initiated time-resolved x-ray absorption spectroscopy. *Annu. Rev. Phys. Chem.* **56,** 221–254 (2005).

39. Chen, L. X. *et al.* MLCT State Structure and Dynamics of a Copper (I) Diimine Complex Characterized by Pump - Probe X-ray and Laser Spectroscopies and DFT Calculations. *J. Am. Chem. Soc.* **125,** 7022–7034 (2003).

40. Chen, L. X. Taking snapshots of photoexcited molecules in disordered media by using pulsed synchrotron x-rays. *Angew. Chem. Int. Ed.* **43,** 2886–2905 (2004).

41. Göries, D. *et al.* Time-resolved pump and probe x-ray absorption fine structure spectroscopy at beamline P11 at PETRA III. *Rev. Sci. Instrum.* **87,** 53116-1-53116–10 (2016).

42. Jesser, A., Rohrmüller, M., Schmidt, W. G. & Herres-Pawlis, S. Geometrical and optical benchmarking of copper guanidine-quinoline complexes: Insights from TD-DFT and many-body perturbation theory. *J. Comput. Chem.* **35,** 1–17 (2014).

43. Chaudhuri, J., Kume, S., Jagur-Grodzinski, J. & Szwarc, M. Chemistry of radical anions of heterocyclic aromatics: I. Electron spin resonance and electronic spectra. *J. Am. Chem. Soc.* **90,** 6421–6425 (1968).

44. Hamm, P., Ohline, S. M. & Zinth, W. Vibrational cooling after ultrafast photoisomerization of azobenzene measured by femtosecond infrared spectroscopy. *J. Chem. Phys.* **106,** 519–529 (1997).

45. Du, L. & Lan, Z. Ultrafast structural flattening motion in photoinduced excited state dynamics of a bis(diimine) copper(I) complex. *Phys. Chem. Chem. Phys.* **18,** 7641–7650 (2016).

46. Westre, T. E. *et al.* A multiplet analysis of Fe K-edge 1s → 3d pre-edge features of iron complexes. *J. Am. Chem. Soc.* **119,** 6297–6314 (1997).

47. Rehr, J. J. & Albers, R. C. Theoretical approaches to x-ray absorption fine structure. *Rev. Mod. Phys.* **72,** 621–654 (2000).

48. Stern, E. A. Theory of the extended x-ray-absorption fine structure. *Phys. Rev. B* **10,** 3027–3037 (1974).

49. Sayers, D. E., Stern, E. A. & Lytle, F. W. New technique for investigating noncrystalline structures: fourier analysis of the extended x-ray-absorption fine structure. *Phys. Rev. Lett.* **27,** 1204–1207 (1971).

50. Czerwieniec, R., Leitl, M. J., Homeier, H. H. H. & Yersin, H. Cu(I) complexes - thermally activated delayed fluorescence. Photophysical approach and material design. *Coord. Chem. Rev.* **325,** 2–28 (2016).

51. Siddique, Z. A.; Yamamoto, Y.; Ohno, T.; Nozaki, K. Structure-Dependent Photophysical

Properties of Singlet and Triplet Metal-to-Ligand Charge Transfer States in Copper(I) Bis(diimine) Compounds, *Inorg. Chem.* **42**, 6366-6378 (2003).

52. Cannizzo, A.; Blanco-Rodríguez, A. M.; Nahhas, A.; Šebera, J.; Záliš, S.; Vlček, A., Jr.; Chergui, M. Femtosecond Fluorescence and Intersystem Crossing in Rhenium(I) Carbonyl-Bipyridine Complexes, *J. Am. Chem. Soc.* **130**, 8967-8974 (2008).

53. Mara, M.W. *et al.* Metalloprotein entatic control of ligand-metal bonds quantified by ultrafast x-ray spectroscopy, *Science* **356**, 1276–1280 (2017).